creative commons
COMMONS DEED

저작자표시-비영리-변경금지 2.0 대한민국

이용자는 아래의 조건을 따르는 경우에 한하여 자유롭게

- 이 저작물을 복제, 배포, 전송, 전시, 공연 및 방송할 수 있습니다.

다음과 같은 조건을 따라야 합니다:

저작자표시. 귀하는 원저작자를 표시하여야 합니다.

비영리. 귀하는 이 저작물을 영리 목적으로 이용할 수 없습니다.

변경금지. 귀하는 이 저작물을 개작, 변형 또는 가공할 수 없습니다.

- 귀하는, 이 저작물의 재이용이나 배포의 경우, 이 저작물에 적용된 이용허락조건을 명확하게 나타내어야 합니다.
- 저작권자로부터 별도의 허가를 받으면 이러한 조건들은 적용되지 않습니다.

저작권법에 따른 이용자의 권리는 위의 내용에 의하여 영향을 받지 않습니다.

이것은 이용허락규약(Legal Code)을 이해하기 쉽게 요약한 것입니다.

Disclaimer

dCollection

이학석사 학위논문

The role of transient eddies in Pacific blocking formation

태평양 블로킹 형성에서의 일시에디의 역할

2019년 2월

서울대학교 대학원

지구환경과학부

황 재 영

The role of transient eddies in Pacific blocking formation
태평양 블로킹 형성에서의 일시에디의 역할

지도 교수 손 석 우

이 논문을 이학석사 학위논문으로 제출함
2018년 10월

서울대학교 대학원
지구환경과학부
황 재 영

황재영의 이학석사 학위논문을 인준함
2018년 12월

위 원 장 _____ (인)

부위원장 _____ (인)

위 원 _____ (인)

Abstract

The mechanism of Pacific blocking formation is investigated by a budget analysis using the quasigeostrophic geopotential tendency equation. In a winter case study, an explosive cyclone exists upstream of the blocking development, and the dynamic relationship between the cyclone and preamplified ridge enables the formation of blocking. Conversely, pre-existing blocking leads to successive blocking formations in a summer case study. These two case studies showed that a large portion of the tendency associated with blocking formation is explained by the tendency derived from the vorticity flux convergence term using the quasigeostrophic geopotential tendency equation. The vorticity flux convergence term is decomposed into high-frequency and low-frequency transient eddies, and the cross-frequency vorticity flux convergence term accounts for a large part of the tendency that is associated with ridge development in the winter case. Particularly, the interaction between the low-frequency flow and high-frequency vorticities is a primary factor in the formation of blocking during the winter 2015. However, the tendency obtained from the

low-frequency vorticity flux term plays a key role in the formation of blocking during the summer 2016. In the composite analysis of the winter and summer seasons, the tendency associated with blocking formation is mainly explained by the tendency calculated from the vorticity flux convergence term, and this result is consistent with the results of the two case studies. The role of the cross-frequency vorticity flux term is dominant in the formation of blocking during the winter season, which is shown in the winter case study. Conversely, the low-frequency vorticity flux term contributions to the formation of blocking are similar to the contributions of the cross-frequency vorticity flux term during the summer season. This result suggests that the dominant mechanism of blocking formation during the winter season is not the same as the dominant mechanism during the summer.

Keyword : blocking, transient eddy, quasi-geostrophic geopotential tendency equation

Student Number : 2016-23149

Table of Contents

1. Introduction

Blocking, which “breaks down” typical westerlies (Rex, 1950), is one of the most important weather phenomena in the mid-latitudes, forming an anomalous large-scale meridional flow. Blocking has both quasistationary and persistent characteristics and usually results in the occurrence of extreme weather events.

During summer, extreme heat waves and catastrophic floods may be related to blocking events (Black et al., 2004; Matsueda, 2011; Hong et al., 2011; Lau and Kim, 2012; Schaller et al. 2018), and blocking may generate extreme cold surges and dry spells during winter (Trigo et al., 2004; Buehler et al., 2011; Jensen 2015; Wang et al., 2015; Luo et al., 2016; Yao et al., 2017; Ma and Zhu, 2018). Additionally, blocking controls the air quality in a region by concentrating air pollutants such as tropospheric ozone and PM10 (Gangoiti et al. 2002; Czernecki et al. 2017).

Several studies have determined factors that can influence the formation of blockings, such as ENSO (Renwick and Wallace, 1996), MJO (Hamill and Kiladis, 2014; Henderson et al., 2016), NAO (Shabbar et al., 2001; Woollings et al., 2008), Arctic amplification

(Francis and Vavrus, 2012; Cohen et al., 2014), and anthropogenic forcings (Dunn-Sigouin and Son, 2013; Masato et al., 2013; Barnes et al., 2014; Woollings et al., 2018). However, the influences of blockings are still inconsistent depending on the literature, and large biases of simulated blockings still remain in the state-of-the-art models (Anstey et al., 2013; Davini and D'Andrea, 2016; Davini et al., 2017). Therefore, improved process understanding and model development are necessary to clarify the relationship (Cohen et al., 2014; Henderson et al., 2016). These difficulties in understanding blocking are due to atmospheric system complexity and inaccuracies in the blocking detection algorithms, but most of the difficulty is derived from the lack of understanding of the blocking formation mechanism, which comprehensively encompasses the entire blocking life-cycle (Woollings et al., 2018).

Many attempts have been made to explain the mechanism of blocking formations. Egger (1978) suggested that nonlinear interactions between slow-moving free waves and standing waves give rise to the formation of blocking. Austin (1980) noted that interference among stationary planetary waves can create an initial state of blocking. Hoskins and Karoly (1981) showed that Rossby

wave propagation induced by tropical forcing can produce block flows. Those studies proposed that stationary or standing waves are associated with the formation of blocking. However, these stationary wave theories use simple models and are insufficient to account for all of the blocking formation cases in real-world.

Reportedly, explosive cyclones are usually observed with blockings, and a possible relationship was confirmed by Berggren et al. (1949), Colucci (1985, 1987), and Tsou and Smith (1990). Additionally, the relationship between blocking and high-frequency transient eddies composed of cyclones and anticyclones were investigated by Shutts (1983, 1986), Holopainen (1987), and Mullen (1987). In several studies, the interaction between synoptic-scale waves (high-frequency eddies) and planetary-scale waves (low-frequency eddies) are the primary factors in blocking formation (Colucci 1985, 1987; Tsou and Smith, 1990; Lupo and Smith, 1995). Furthermore, Nakamura et al. (1997) noted that the primary factors of blocking formation are different according to region. Recently, Nakamura and Huang (2018) showed that stationary waves regulate the capacities of transient eddies in the jet stream and determine the formation of blocking.

Most previous studies that investigated the blocking mechanism focused on the boreal winter season. In particular, these studies tended to target blockings in the Euro–Atlantic region. Moreover, some case studies or composite analyses over the Euro–Atlantic region were performed to investigate the mechanism of blocking formation in summer (Lupo et al., 2012; Drouard and Woollings, 2018). Studies on Pacific blocking have not been conducted much in comparison with those in the Euro–Atlantic region. In particular, the mechanism of Pacific blocking in summer was investigated by only a few studies.

The mechanism of Pacific blocking formation during summer was reported by Nakamura and Fukumachi (2004). The authors showed that the blocking formation mechanism over the Okhotsk region differs with regard to occurrence time and reported that the eddy forcing does not play a crucial role in the formation of blocking past July, and the local breaking propagation of the stationary Rossby wave packet leads to the formation of blocking. Since the researchers focused on blocking over the Okhotsk region in July, it is necessary to investigate a more comprehensive perspective for Pacific blocking formation in summer.

In this study, we focus on the role of transient eddies in Pacific blocking formation using the quasigeostrophic geopotential tendency equation. We revisit the evidence showing that high-frequency transient eddy forcing is a key factor in the Pacific blocking formation in winter, which was reported by Nakamura et al. (1997). Similarly, the mechanism of blocking formation in summer is also investigated.

The quasigeostrophic tendency equations and blocking algorithm used in this study are introduced in Section 2. To investigate the detailed blocking dynamics, case studies for the summer and winter are conducted and outlined in Section 3. In Section 4, a composite analysis is conducted for the summer and winter to more comprehensively consider our results from Section 3. Finally, our findings derived from Sections 3 and 4 are comprehensively discussed in Section 5.

2. Data and Method

2.1. Hybrid Index

Many previous studies have used various indices to investigate the phenomena related to blocking or blocking itself. In general, the variables used to detect blocking are geopotential height (Dole and Gordon, 1983; Tibaldi and Molteni, 1990; Barriopeddro et al., 2010; Dunn-Sigouin et al., 2013) and potential vorticity (Pelly and Hoskins 2003; Masato et al., 2013). In addition, even if the same variable is used to detect blockings, several analytical methods have been used in the literature, such as the anomalous field method (Dole and Gordon, 1983), the absolute field method (Tibaldi and Molteni, 1990), and the hybrid method (Barriopeddro et al., 2010; Dunn-Sigouin et al., 2013).

Although each blocking detection algorithm captures the blocking features well and qualitatively shows similar results in annual blocking climatology regardless of variables and methodology (Barnes et al., 2012), the results obtained from each algorithm with different dimensionality are quantitatively different

(Barriopeddro et al., 2010), especially in terms of seasonal climatology.

In this paper, the Dunn-Sigouin et al. (2013) index, which is a hybrid index, is chosen to detect Pacific blocking. This method is particularly useful in detecting omega-shaped blockings rather than the classic Tibaldi and Molteni (1990) index. Our research focuses on the formation of blocking on the hourly time scale, and thus, this index, which is based on daily mean data to identify the blocking, must be slightly modified for our purposes. The modified procedures of detecting Pacific blocking are as follows:

1) The geopotential height anomaly Z' is defined to as

$$Z' = Z - \bar{Z} - \hat{Z} \qquad (1)$$

where Z is normalized geopotential height at 500 hPa, $\bar{Z}$ is the running annual mean of Z centered on a given hour, and $\hat{Z}$ is a mean seasonal cycle of running monthly mean of $Z - \bar{Z}$ centered on a given hour.

2) The anomaly (Z'), which is greater than 1.5 standard deviations of the hemispheric mean of Z', is referred to as blocking anomalies and expressed as a closed contour.

3) It is selected that blocking anomalies satisfy the spatial threshold ($2.5 \times 10^6\ km^2$).

4) The overlap ratio of the contours that continuously exist in 6-hour intervals should be 0.7 or more.

5) The contour has an area that shows at least meridional geopotential height reversal.

6) The blocking anomalies that satisfied the above conditions must exist for at least 5 consecutive days in the Pacific domain ($120°\mathrm{E} - 250°\mathrm{E}$).

2.2. QG tendency equations and transient eddies

A quasigeostrophic geopotential tendency equation is adopted to determine the formation of blocking. From the vorticity equation and thermodynamic energy equation, we can derive the quasigeostrophic geopotential tendency equation.

$$\frac{\partial \zeta}{\partial t} = -V \cdot \nabla(\zeta + f) + f\frac{\partial \omega}{\partial p} \quad (2)$$

$$\frac{\partial \theta}{\partial t} = -V \cdot \nabla\theta - \frac{\partial \theta}{\partial p}\omega \quad (3)$$

where ζ is relative vorticity, θ is potential temperature, f is Coriolis parameter, V is horizontal wind, and ω is pressure

velocity.

By dividing the static stability parameter ($s \equiv -\frac{\partial\theta}{\partial p}$), Eq. (3) can be written as follows:

$$\frac{1}{s}\frac{\partial\theta}{\partial t} = -\frac{1}{s}V\cdot\nabla\theta + \omega \quad (4)$$

By eliminating the ω term with some manipulation of Eq. (3) and Eq. (4), we can rewrite the equations as follows:

$$\frac{\partial\zeta}{\partial t} - f\frac{\partial}{\partial p}\left(\frac{1}{s}\frac{\partial\theta}{\partial t}\right) = f\frac{\partial}{\partial p}\left(\frac{1}{s}V\cdot\nabla\theta\right) - V\cdot\nabla(\zeta+f) \quad (5)$$

By assuming $\mathrm{V(horizontal\ wind)} = V_g$, $f(Coriolis\ parameter) = f_o$, $\theta = \theta_o(p,t) + \theta_d(x,y,p,t)$, and $s \approx s_O \equiv -\frac{\partial\theta_o}{\partial p}$, Eq. (5) can be written as follows:

$$\left\{\frac{1}{f_o}\nabla^2 + f_o\frac{\partial}{\partial p}\left(\frac{1}{s_o}\frac{P}{R}\left(\frac{p_o}{p}\right)^{\frac{R}{C_p}}\frac{\partial}{\partial p}\right)\right\}\frac{\partial\phi}{\partial t} = -\nabla\cdot V(\zeta+f) + f_o\frac{\partial}{\partial p}\left(\nabla\cdot\frac{V\theta_d}{s_o}\right) \quad (6)$$

where s_O is the hemispheric mean static stability, f_o is the Coriolis parameter at 45^oN, R is the gas constant, p_O is the constant pressure at 1000 hPa, p is the pressure, θ_d is the potential temperature deviation from the hemispheric mean potential temperature, and C_p is the specific heat capacity.

To solve the Eq. (6), thermodynamic energy equation is applied as a boundary condition, as in Lau and Holopainen (1984).

$$-\frac{p}{R}\left(\frac{p_o}{p}\right)^{\frac{R}{C_p}}\frac{\partial}{\partial p}\left(\frac{\partial \phi}{\partial t}\right)_{BC}^{heat} = f_o \frac{\partial}{\partial p}\left(\frac{1}{s_o}\nabla \cdot \left(V\,\theta_d\right)\right) \quad (7)$$

$$\frac{\partial}{\partial p}\left(\frac{\partial \phi}{\partial t}\right)_{BC}^{vort} = 0 \quad (8)$$

The superscription in Eq. (7) and Eq. (8) means that the boundary conditions are calculated to form differential divergence of heat flux and divergence of vorticity flux, respectively. Additionally, a sensitivity test of the boundary condition is also conducted, such as the slip boundary condition (i.e., $-\frac{p}{R}\left(\frac{p_o}{p}\right)^{\frac{R}{C_p}}\frac{\partial}{\partial p}\left(\frac{\partial \phi}{\partial t}\right)_{BC}^{heat} = 0$). The difference between the results obtained from two boundary conditions is negligible at 500 hPa, which was also reported by Tsou and Smith (1990).

To investigate the role of transient eddies in the formation of blocking, the transient eddies must be defined. We defined high-frequency transient eddies as 165 weight 8-day high-pass Lanczos filtered data, and low-frequency transient eddies are defined as unfiltered data minus high-frequency transient eddies. For the convenience of considering the forcing term, Eq. (6) can be written simply as follows:

$$\left\{\frac{1}{f_o}\nabla^2 + f_o \frac{\partial}{\partial p}\left(\frac{1}{s_o}\frac{P}{R}\left(\frac{p_o}{p}\right)^{\frac{R}{C_p}}\frac{\partial}{\partial p}\right)\right\}\frac{\partial \phi}{\partial t} = F^{\,vort} + F^{\,heat} \quad (9)$$

Here, we express the $-\nabla \cdot V(\zeta + f)$ term in the RHS of Eq. (6) as the vorticity forcing term (F^{vort}) and the $f_o \frac{\partial}{\partial p}\left(\nabla \cdot \frac{V\theta_d}{s_o}\right)$ term in the RHS of Eq. (6) is referred to as the heat forcing term (F^{heat}). To examine the contribution of transient eddies to the formation of blocking, we must decompose the forcing terms as follows:

$$F^{heat} = f_o \frac{\partial}{\partial p}\left(\frac{1}{s_o}\nabla \cdot \left(V_{HF}\,\theta_{d\cdot HF} + V_{LF}\,\theta_{d\cdot LF} + V_{HF}\,\theta_{d\cdot LF} + V_{LF}\,\theta_{d\cdot HF}\right)\right) \quad (10)$$

$$F^{vort} = -\nabla \cdot (V_{HF}\zeta_{HF} + V_{LF}\zeta_{LF} + V_{HF}\zeta_{LF} + V_{LF}\zeta_{HF} + V_{HF}f + V_{LF}f) \quad (11)$$

For brevity, forcing term abbreviations and the tendency of the forcing term are derived from the quasigeostrophic geopotential tendency equation and presented in Table 1.

2.3. Data

In this study, 6-hour data from the European Centre for Medium-Range Weather Forecasts Interim reanalysis (Dee et al., 2011) are used to detect Pacific blockings and determine their formation mechanism for 1979-2016. To detect the blockings, 500-hPa geopotential height (Z500) fields are applied, and sea-level pressure is used to investigate the features of surface

cyclones associated with the formation of blocking. To calculate the quasigeostrophic geopotential tendency equations, 13 vertical levels of horizontal winds, relative vorticity, and temperature are used. All data used in this paper are interpolated into $2.5^o \times 2.5^o$ lat.−long. grids, and we confirm that our results are insensitive to the resolution.

3. Case Studies

3.1. Winter

The blocking that occurred on 1800 UTC 21 February 2015 (140^oW) was chosen for the winter case study. Figure 1 shows the Z500 fields associated with the formation of blocking for 1800 UTC 17 February 2015–1800 UTC 21 February 2015. At 1800 UTC 17 February 2015, 4 days before the onset, an amplified planetary-scale ridge associated with a positive geopotential height anomaly exists over the eastern Pacific ($50^oN, 130^o$W), and a synoptic-scale trough related to a surface cyclone in the upstream region was moving eastward (Figure 1a).

The pre-existing positive geopotential height anomaly over the east Pacific gradually decayed, and another positive geopotential height anomaly began to grow in the downstream region of the synoptic-scale trough at 0600 UTC 19 February 2015 (Figure 1d). From 0600 UTC 20 February 2015, 48 hours before the onset, the intensity of the surface cyclone was remarkably weakened, and the cyclone began to move northward along the

ridge. Simultaneously, the newly developing positive anomaly began to rapidly grow and expand (Figures 2f–2i). At the onset (1800 UTC 21 February 2015), the positive anomaly created a meridionally elongated large–scale ridge, which generated an extreme dipole pattern over North America in association with an extreme cold wave over the eastern American regions (Jensen 2015; Wang et al. 2015; Singh et al. 2016). Another synoptic–scale trough linked with a surface cyclone moved into the upstream area of the weakened surface cyclone that was moving northward along the ridge (Figure 1i). A synoptic–scale disturbance can induce large–scale ridge amplification, and the dynamic behavior of the disturbance is related to the formation of blocking. The results are similar to those reported by Colucci (1985, 1987), Tsou and Smith (1990), and Lupo and Smith (1995), and this feature can be seen in an idealized model experiment (Swanson, 2000).

To focus on blocking ridge development, the tendency calculated from observations at 72 hours (3 days), 48 hours (2 days), and 24 hours (1 day) before onset and the quasigeostrophic geopotential tendency equation described above are depicted in Figure 2. A positive tendency was observed in the developing ridge

in association with the formation of blocking, and the tendency significantly increased 2 days prior to the onset of blocking.

The height tendency shows a dipole pattern in the upstream regions due to the eastward movement of the trough (Figures 2a, 2e, 2i). The tendency obtained from the quasigeostrophic geopotential tendency equation is qualitatively similar to that calculated from the observations. Additionally, the tendency derived from the quasigeopotential tendency equation captures the tendency trend associated with the blocking ridge and trough in the upstream area (Figures 2b, 2f, 2j). This trend reveals that a large part of the tendency over the developing ridge area is explained by the vorticity forcing term (Figures 2c, 2g, 2k), and the trend is also similar to the total tendency ($\chi^{total} = \chi^{vort} + \chi^{heat}$). This result is consistent with the results of Colucci (1985) and Tsou and Smith (1990). On the other hand, this finding shows that the contribution of the heat forcing term is somewhat minor in comparison to the developing blocking ridges (Figures 2d, 2h, 2i).

Figure 3 reveals the tendency calculated from each transient eddy forcing term in Eq. (11). The contribution of cross-frequency relative vorticity forcing terms ($-\nabla \cdot (V_{LF}\zeta_{HF} + V_{HF}\zeta_{LF})$) to the

tendency derived from vorticity forcing (χ^{vort}) is confirmed to be dominant (Figures 3d, 3h, 3l). However, the tendency obtained by the high-frequency vorticity forcing terms ($-\nabla \cdot (V_{HF}\zeta_{HF} + V_{HF}f)$) and low-frequency vorticity forcing terms ($-\nabla \cdot (V_{LF}\zeta_{LF} + V_{LF}f)$) are minor factors in the formation of blocking (Figures 3b, 3c, 3f, 3g, 3j, 3k). Notably, the cross-frequency forcing term, which represents the interactions between different scales, is a primary factor in the formation of blocking.

The tendency calculated from each forcing term in Eq. (11) to elucidate the role of transient eddies associated with blocking formation 1 day prior to the onset of blocking is shown in Figure 4. Figures 4a and 4b illustrate the tendency ($\chi^{vort}_{HF\_R}$) derived from the high-frequency relative vorticity forcing ($-\nabla \cdot V_{HF}\zeta_{HF}$) and the tendency ($\chi^{vort}_{HF\_P}$) derived from the high-frequency planetary vorticity forcing ($-\nabla \cdot V_{HF}f$).

As shown in Figure 3j, the contribution of $\chi^{vort}_{HF\_P}$ and $\chi^{vort}_{HF\_R}$ is negligible. Figures 4c and 4d show $\chi^{vort}_{CF\_1}$ and $\chi^{vort}_{CF\_2}$ respectively of which signs are opposing (Figures 4c, 4d), and the magnitudes are somewhat different. The overall pattern of χ^{vort}_{CF} ($=\chi^{vort}_{CF\_1} + \chi^{vort}_{CF\_2}$) is shown in Figure 4d, and in particular, the tendency associated with

the developing ridge is explained by $\chi_{CF\_1}^{vort}$. The tendency obtained from the low-frequency absolute vorticity forcing term ($-\nabla \cdot (V_{LF}\zeta_{LF} + V_{LF}f)$) is shown in Figures 4e and 4f. The magnitudes of $\chi_{LF\_P}^{vort}$ and $\chi_{LF\_R}^{vort}$ are comparable to those of the cross-frequency vorticity forcing terms, but the total contribution of the low-frequency forcing term is small due to those compensating feature of the forcing terms (Figures 4e, 4f).

This result suggests that the tendency calculated from the cross-frequency vorticity forcing term plays a key role in the tendency related to the formation of blocking; this role is especially true for the $-\nabla \cdot V_{LF}\zeta_{HF}$ term, which physically means that interactions between the slowly varying background flow (or planetary-scale flow) and high-frequency relative vorticity (or synoptic-scale disturbance) are primary factors in the formation of blocking. It is consistent with the results obtained by Tsou and Smith (1990), Colucci (1985, 2001), and Nakamura and Huang (2018). Nakamura et al. (1997) reported that high-frequency transient eddy forcing plays a crucial role in Pacific blocking formation, and the result seems to be in contrast to our result. However, we note that this discrepancy in the results is due to the

definition of transient eddies. Nakamura et al. (1997) defined the high-frequency transient eddy as the sum of the cross-frequency transient eddy and high-frequency transient eddy in our definitions, so their finding is also consistent with our results.

To compare the features between the transient forcing term and its tendency, we reveal the transient eddy forcing term in Eq. (11) 1 day before the onset, which are shown in Figure 5. Although the magnitude of $-\nabla \cdot V_{HF} f$ is dominant (Figure 5b), the tendency ($\chi^{vort}_{HF\_P}$) accounts for the minor portion of the total tendency (Figure 4). The pattern and magnitude of $\chi^{vort}_{LF\_P}$ are comparable to $\chi^{vort}_{LF\_R}$ (Figures 4e, 4f). However, when considering the forcing terms, their relationship could no longer be found (Figures 5e, 5f). On the other hand, only cross-frequency vorticity forcing terms with a negligible magnitude explain the total tendency over the developing ridge (Figures 5c, 5d).

As a result, the forcing terms could not represent the shape or magnitude of the geopotential height tendency, but the forcing terms can directly contribute to the tendency of quasigeostrophic potential vorticity in terms of quasigeostrophic potential vorticity equation. The reason for this discrepancy between the geopotential

height tendency and the forcing term can be found in the relationship between them. Potential vorticity in the quasigeostrophic approximation is regarded as a function of the geopotential Laplacian term, which means the relationship between the geopotential height and forcing term should be considered the curvature of the forcing term or its scale (Hoskins et al., 1985).

3.2. Summer

The blocking that occurred on 1800 UTC 16 July 2016 (150^oW) was chosen for the summer case study. Figure 6 shows the Z500 fields associated with the formation of blocking for 1800 UTC 12 July 2016–1800 UTC 16 July 2016. At 1800 UTC 12 July 2016, 4 days before the onset, blocking existed over the Okhotsk region ($50^oN, 170^oE$), which gave rise to anomalous coolness over Japan (Nakamura and Fukumachi, 2004), and the surface cyclone developed over the downstream region of the blocking (Figure 6a).

Over time, development of the surface cyclone gives rise to trough deepening over the eastern Pacific ($50^oN, 160^oW$), and the cyclone decayed rapidly (Figures 6b–6d). At 1800 UTC 14 July

2016, 48 hours before the onset, the surface cyclone occurred over the trough, and the positive geopotential height anomaly began to notably develop over $50^oN, 140^oW$ (Figure 6e). From 0600 UTC 15 July 2016, the surface cyclone linked to the trough in the upstream region also began to rapidly develop, and the positive height anomaly became quasistationary and the magnitude significantly increased (Figures 6f–6i). On the other hand, the previous blocking decayed with an eastward shift along the westerly flow, and the blocking is absorbed by the newly developed blocking over the eastern Pacific after 1800 UTC 16 July 2016 (not shown). As shown by summer blocking case in Figure 6, the previous blocking can lead the successive blocking during summer (Mukougawa and Sato, 1999).

As shown in Figure 2, the tendency calculated from the observations at 72 hours (3 days), 48 hours (2 days), and 24 hours (1 day) before onset and the quasigeostrophic geopotential tendency equation described above are displayed in Figure 7. A positive tendency was observed in the developing ridge in association with the formation of blocking, and a negative geopotential height tendency in the deepening trough was observed.

Additionally, there appears to be a height tendency dipole pattern in the high-latitude area (80^oN) due to the eastward movement of the trough (Figures 7a, 7e, 7i). This feature is similar to that of the case study in winter. The tendency obtained from the quasigeostrophic geopotential tendency equation is qualitatively similar to that calculated from the observations. Additionally, the tendency derived from the quasigeopotential tendency equation accurately captures the tendency trend associated with the blocking ridge and trough in the upstream area (Figures 7b, 7f, 7j). A large part of the tendency over the developing ridge area is explained by the vorticity forcing term (Figures 7c, 7g, 7k), and the trend is also similar to the total tendency ($\boldsymbol{\chi}^{total}$). On the other hand, the contribution of the heat forcing term is somewhat minor over the developing blocking ridges (Figures 7d, 7h, 7i). In both the summer and winter case studies, most of the geopotential height tendency associated with the formation of blocking can be explained by the vorticity forcing term.

To examine the role of transient eddies in summer blocking formation, the tendency is calculated from each transient eddy forcing term in Figure 8. The contribution of $(-\nabla \cdot (V_{LF}\zeta_{HF} + V_{HF}\zeta_{LF}))$

to the tendency associated with the developing ridge is confirmed to be minor (Figures 8d, 8h, 8l). Additionally, the tendency obtained by the high-frequency vorticity forcing terms ($-\nabla \cdot (V_{HF}\zeta_{HF} + V_{HF}f)$) remains small (Figures 8b, 8f, 8j). In contrast, the low-frequency vorticity forcing terms ($-\nabla \cdot (V_{LF}\zeta_{LF} + V_{LF}f)$) account for a large portion of the tendency in the formation of blocking (Figures 8c, 8g, 8k). This finding suggests that the blocking formation dynamics in winter may not be the same in summer.

In order to elucidate the role of transient eddies associated with the formation of blocking, the tendency calculated from each forcing term in Eq. (11), at 1 day before the onset, is shown in Figure 9. Figures 9a and 9b depict the tendency ($\chi^{vort}_{HF\_R}$) obtained from $-\nabla \cdot V_{HF}\zeta_{HF}$ and the tendency ($\chi^{vort}_{HF\_P}$) derived from $-\nabla \cdot V_{HF}f$. Although $\chi^{vort}_{HF\_P}$ accounts for a large part of χ^{vort}_{HF}, the tendencies in Figures 9a and 9b remain negligible, and it is consistent with the winter case in Figure 9j. Figures 9c and 9d show $\chi^{vort}_{CF\_1}$ and $\chi^{vort}_{CF\_2}$, respectively, and the signs are opposing. The overall magnitude is somewhat different between the two terms, but the tendency magnitude associated with the formation of blocking compensates for each term (Figures 9c-9d). The tendencies obtained from the

low−frequency absolute vorticity forcing terms ($-\nabla\cdot(V_{LF}\zeta_{LF}), -\nabla\cdot(V_{LF}f)$) are shown in Figures 9e and 9f, respectively. The total tendency over the blocking ridge is explained by the sum of the low−frequency absolute vorticity forcing.

Figure 10 shows the transient eddy forcing term at 1 day before the onset for comparison to the forcing term and its tendency. As shown in Figure 9b, the $-\nabla\cdot V_{HF}f$ magnitude is dominant, but the contribution of its tendency ($\chi^{vort}_{HF\_P}$) to the total tendency is minor (Figure 10b). The pattern and magnitude of $\chi^{vort}_{CF\_1}$ are comparable to those of $\chi^{vort}_{CF\_2}$ (Figures 9c, 9d) in the region in relation to the formation of blocking, but these features are difficult to find in Figures 10c and 10d. On the other hand, the contribution to the formation of blocking $\chi^{vort}_{LF\_P}$ is similar to that of $\chi^{vort}_{LF\_R}$, but the magnitude of $-\nabla\cdot V_{LF}f$ is much larger than that of $-\nabla\cdot V_{LF}\zeta_{LF}$ (Figures 10e, 10f). Based on the results, we confirm that the forcing term cannot represent the geopotential height tendency.

4. Composite Studies

In previous sections, blocking dynamics were indicated to potentially be different by season. However, these results were determined based on the case study, so findings may depend on the blocking case (Tracton, 1990). Thus, we need to conclude our results more comprehensively by performing a composite analysis.

In the previous study, a composite analysis was performed based on blocking genesis regions (Nakamura et al. 1997, Nakamura and Fukumachi, 2004; Drouard and Woollings, 2018), or the analysis was conducted with different reference areas defined by the dynamic blocking features (Nakamura and Huang, 2018). In this study, we obtain a composite of the geopotential height anomaly field in winter (summer) by using the Z500 anomaly fields at each blocking onset, and we define the reference latitude of the winter (summer) season as the grid point showing a maximum value of composite anomaly. We refer to 47.5^oN (52.5^oN) as the reference latitude for the winter (summer) season in association with Pacific blocking. This result is similar to the reference latitude defined by Pelly and Hoskins (2003), which was calculated from eddy kinetic

energy, and the researchers also showed that the reference latitude is seasonally dependent. We also calculate the reference latitude by calculating eddy kinetic energy at 500 hPa, as reported by Pelly and Hoskins (2003), and our reference latitude is similar to that obtained by their definition (not shown). We refer to the blocking center as the grid point that shows the maximum value of geopotential height anomaly, and each blocking center which is moved to the reference latitude by using the parallel translation is averaged based on its center. For the sharpness of composite analysis, we exclude the blockings of which contour does not contain reference latitude. As can be seen from the two case studies, it is due to the fact that the geopotential height anomaly associated with the blocking onset begins to develop rapidly 48 hours before. Thus, we conducted a composite analysis from 48 hours before the blocking formation onset. Additionally, the parallel translation applied to the blocking onset is used to composite each blocking case before the onset. The number of composited samples is 73 (39) in winter (summer).

For statistical significance, the bootstrap resampling method is selected, and the confidence intervals are calculated by

replicating the mean from the original samples 10,000 times, which involves sampling duplication.

Figure 11 depicts a composite of the winter blocking formation. The time evolution of the Z500 field composite which is related to the formation of blocking at 12-hour intervals is shown in Figures 11a-11d. Over time, the composite blocking ridge is gradually developed, and the trough in the upstream area becomes increasingly deeper (Figures 11e-11h).

The time series of geopotential height tendency is related to the blocking development obtained from the geopotential tendency equation (Figure 12a), and the transient eddy contributions to the tendency are calculated (Figure 12b). These values are obtained by averaging the quantities within the second grid of the grid point where the maximum positive tendency is seen in the observations, and the tendency derived from the equation is also calculated by using the same grid points that were used in the observations.

The tendency obtained by the equation captures the observations well, and the contribution of the vorticity forcing to the total tendency is dominant. Moreover it is shown that the vorticity forcing trend is similar to the trend of the observations. In contrast,

the tendency obtained from the heat forcing is small (Figure 12a). These results are shown in our case study and are consistent with the results of previous studies reported by Colucci (1985) and Tsou and Smith (1990).

To investigate the role of transient eddies in blocking formation, the tendency derived from the vorticity forcing term is decomposed into $\boldsymbol{\chi_{CF}^{vort}}$, $\boldsymbol{\chi_{HF}^{vort}}$, and $\boldsymbol{\chi_{LF}^{vort}}$ (Figure 12b). $\boldsymbol{\chi_{CF}^{vort}}$ not only occupies most of the total tendency but also captures the fluctuation of the total tendency. In contrast, the contribution of $\boldsymbol{\chi_{LF}^{vort}}$ and $\boldsymbol{\chi_{HF}^{vort}}$ is significantly smaller than that of $\boldsymbol{\chi_{CF}^{vort}}$. This result is consistent with the winter case study (Figure 3).

The same analysis is performed on the summer blockings. Figure 13 shows the evolution of the blocking composite in summer. The time evolution of the Z500 field composite related to blocking formation at 12-hour intervals is shown in Figures 13a-13d. Over time, the composite blocking ridge is gradually developing, and the trough in the upstream becomes increasingly deeper (Figures 13e-13h). It is also shown that the tendency magnitude and block size are smaller than the winter blocking composite.

The tendency related to blocking formation during summer is shown in Figure 14. As shown in Figure 13a, the tendency calculated by the vorticity forcing accounts for a large part of the blocking development (Figure 14a). Figure 14b shows the role of transient eddy forcing in the summer blocking formation. In contrast to winter, the contribution of $\boldsymbol{\chi_{CF}^{vort}}$ to the total tendency ($\boldsymbol{\chi^{vort}}$) is similar to that of $\boldsymbol{\chi_{LF}^{vort}}$, but the magnitude of $\boldsymbol{\chi_{HF}^{vort}}$ is significantly smaller than the other tendencies. This result suggests two possibilities. One possibility is that most of the blockings in summer can be explained by the combination of cross-frequency forcing and low-frequency forcing. The other possibility is that there are two blocking categories that can be dominantly explained by a cross-frequency forcing and low-frequency forcing, respectively.

5. Summary and Discussion

In this study, two case studies and a composite study are conducted to investigate seasonal differences in the role of transient eddies in Pacific blocking formation by calculating the quasigeostrophic geopotential tendency. The tendency derived from the vorticity forcing plays a key role in Pacific blocking formation despite the season, and our results are consistent with those of Colucci (1985), Tsou and Smith (1990).

To elucidate the role of transient eddies in blocking formation, the vorticity forcing term decomposed by time-filtered quantities is calculated using the tendency equation. The contribution of cross-frequency forcing terms to total tendency is dominant in winter. In particular, the cross-frequency relative vorticity forcing term associated with low-frequency filtered background wind and high-frequency filtered vorticity is a crucial factor in Pacific blocking formation. This finding suggests that the wave interaction between synoptic-scale waves and planetary-scale waves is a primary factor for the formation of Pacific blocking in winter, and this result is similar to previous studies which are

targeted Euro-Atlantic blocking (Lupo and Smith, 1995) or used different equations (Nakamura and Huang, 2018).

However, the contributions of low-frequency vorticity forcing and cross-frequency vorticity forcing to summer blocking formation are similar. This composite result should be interpreted with caution because the significant tendency intervals derived from the low-frequency vorticity forcing and cross-frequency vorticity forcing overlap each other. For winter, the ascendancy of the contributions of the transient eddy forcing terms to the total tendency is determined by conducting the statistical significance test. On the other hand, the contribution of the low-frequency vorticity forcing term is similar to that of the cross-frequency vorticity forcing term, and thus, it is difficult to examine the ascendancy between those terms in each blocking case in summer. Thus, there are two possible interpretations of the composite result, especially for summer. One possible interpretation is that most of the summer blocking cases show similar contributions between the cross-frequency vorticity forcing and low-frequency vorticity forcing to the blocking formation. The other possible interpretation is that there are two blocking categories that can be dominantly

explained by the cross-frequency forcing and low-frequency forcing, respectively. Thus, further work must be performed to eliminate the results misinterpretation, and we suspect that there are two blocking categories with different dynamics in summer.

Notably, the geopotential height is closely related to the potential vorticity (or relative vorticity) in the quasigeostrophic approximation. However, in regard to examining this relationship through quantitative analysis, the scale or wavenumber of potential vorticity (or relative vorticity) must be considered. Thus, the results must be interpreted with caution depending on which variables are used to investigate the blocking dynamics in the literature.

Bibliography

Anstey, J. A., and Coauthors, 2013: Multi-model analysis of Northern Hemisphere winter blocking: Model biases and the role of resolution. *J. Geophys. Res. Atmos.*, doi:10.1002/jgrd.50231.

Austin, J. F., 1980: The blocking of middle latitude westerly winds by planetary waves. *Q. J. R. Meteorol. Soc.*, doi:10.1002/qj.49710644807.

Barnes, E. A., J. Slingo, and T. Woollings, 2012: A methodology for the comparison of blocking climatologies across indices, models and climate scenarios. *Clim. Dyn.*, doi:10.1007/s00382-011-1243-6.

_____, E. Dunn-Sigouin, G. Masato, and T. Woollings, 2014: Exploring recent trends in Northern Hemisphere blocking. *Geophys. Res. Lett.*, doi:10.1002/2013GL058745.

Barriopedro, D., R. García-Herrera, and R. M. Trigo, 2010: Application of blocking diagnosis methods to General Circulation Models. Part I: A novel detection scheme. *Clim. Dyn.*, doi:10.1007/s00382-010-0767-5.

Berggren, R., B. Bolin, and C.-G. Rossby, 1949: An Aerological Study of Zonal Motion, its Perturbations and Break-down. *Tellus*, doi:10.1111/j.2153-3490.1949.tb01257.x.

Black, E., M. Blackburn, G. Harrison, B. Hoskins, and J. Methven, 2004: Factors contributing to the summer 2003 European heatwave. *Weather,* **59,** 217-223

Buehler, T., C. C. Raible, and T. F. Stocker, 2011: The relationship of winter season North Atlantic blocking frequencies to extreme cold or dry spells in the ERA-40. *Tellus, Ser. A Dyn. Meteorol. Oceanogr.*, doi:10.1111/j.1600-0870.2010.00492.x.

Cohen, J., and Coauthors, 2014: Recent Arctic amplification and extreme mid-latitude weather. *Nat. Geosci.*, doi:10.1038/ngeo2234.

Colucci, S. J., 1985: Explosive Cyclogenesis and Large-Scale Circulation Changes: Implications for Atmospheric Blocking. *J. Atmos. Sci.*, **42**, 2701-2717, doi:10.1175/1520-0469(1985)042<2701:ECALSC>2.0.CO;2.

_____, 1987: Comparative Diagnosis of Blocking Versus Nonblocking Planetary-Scale Circulation Changes during Synoptic-Scale Cyclogenesis. *J. Atmos. Sci.*, **44**, 124-139,

_____, 2001: Planetary-Scale Preconditioning for the Onset of Blocking. *J. Atmos. Sci.*, doi:10.1175/1520-0469(2001)058<0933:PSPFTO>2.0.CO;2.

Czernecki, B., M. Półrolniczak, L. Kolendowicz, M. Marosz, S. Kendzierski, and N. Pilguj, 2017: Influence of the atmospheric conditions on PM10concentrations in Poznań, Poland. *J. Atmos. Chem.*, **74**, 115-139, doi:10.1007/s10874-016-9345-5.

Davini, P., and F. D'Andrea, 2016: Northern Hemisphere atmospheric blocking representation in global climate models: Twenty years of improvements? *J. Clim.*, doi:10.1175/JCLI-D-16-0242.1.

_____, and Coauthors, 2017: Climate SPHINX: Evaluating the impact of resolution and stochastic physics parameterisations in the EC-Earth global climate model. *Geosci. Model Dev.*, doi:10.5194/gmd-10-1383-2017.

Dee, D. P., and Coauthors, 2011: The ERA-Interim reanalysis: Configuration and performance of the data assimilation system. *Q. J. R. Meteorol. Soc.*, doi:10.1002/qj.828.

Dole, R. M., and N. D. Gordon, 1983: Persistent Anomalies of the Extratropical Northern Hemisphere Wintertime Circulation: Geographical Distribution and Regional Persistence Characteristics. *Mon. Weather Rev.*, doi:10.1175/1520-0493(1983)111<1567:PAOTEN>2.0.CO;2.

Drouard, M., and T. Woollings, 2018: Contrasting Mechanisms of Summer Blocking Over Western Eurasia. 40–48, doi:10.1029/2018GL079894.

Dunn–Sigouin, E., and S. W. Son, 2013: Northern Hemisphere blocking frequency and duration in the CMIP5 models. *J. Geophys. Res. Atmos.*, **118**, 1179–1188, doi:10.1002/jgrd.50143.

_____, S.–W. Son, and H. Lin, 2013: Evaluation of Northern Hemisphere Blocking Climatology in the Global Environment Multiscale Model. *Mon. Weather Rev.*, doi:10.1175/MWR–D–12–00134.1.

Egger, J., 1978: Dynamics of Blocking Highs. *J. Atmos. Sci.*, doi:10.1175/1520–0469(1978)035<1788:DOBH>2.0.CO;2.

Francis, J. A., and S. J. Vavrus, 2012: Evidence linking Arctic Amplification to Extreme Weather.pdf. *Geophys. Res. Lett.*, doi:10.1029/2012GL051000.

Gangoiti, G., and Coauthors, 2002: Regional transport of pollutants over the Bay of Biscay: Analysis of an ozone episode under a blocking anticyclone in west–central Europe. *Atmos. Environ.*, **36**, 1349–1361, doi:10.1016/S1352–2310(01)00536–2.

Hamill, T. M., and G. N. Kiladis, 2014: Skill of the MJO and Northern Hemisphere Blocking in GEFS Medium-Range Reforecasts. *Mon. Weather Rev.*, doi:10.1175/MWR-D-13-00199.1.

Henderson, S. A., E. D. Maloney, and E. A. Barnes, 2016: The influence of the Madden-Julian oscillation on Northern Hemisphere winter blocking. *J. Clim.*, **29**, 4597-4616, doi:10.1175/JCLI-D-15-0502.1.

Holopainen, E., and C. Fortelius, 1987: High-Frequency Transient Eddies and Blocking. *J. Atmos. Sci.*, doi:10.1175/1520-0469(1987)044<1632:HFTEAB>2.0.CO;2.

Hong, C., 2011: Roles of European blocking and tropical-extratropical interaction in the 2010 Pakistan flooding. *Geophys. Res. …*, doi:10.1029/2011GL047583.

Hoskins, B. J., and D. J. Karoly, 1981: The Steady Linear Response of a Spherical Atmosphere to Thermal and Orographic Forcing. *J. Atmos. Sci.*, doi:10.1175/1520-0469(1981)038<1179:TSLROA>2.0.CO;2.

_____, M. E. McIntyre, and A. W. Robertson, 1985: On the use and significance of isentropic potential vorticity maps. *Q. J. R. Meteorol. Soc.*, doi:10.1002/qj.49711146602.

Jensen, A. D., 2015: A dynamic analysis of a record breaking winter season blocking event. *Adv. Meteorol.*, **2015**, doi:10.1155/2015/634896.

Lau, N.-C., and E. O. Holopainen, 1984: Transient Eddy Forcing of the Time-Mean Flow as Identified by Geopotential Tendencies. *J. Atmos. Sci.*, doi:10.1175/1520-0469(1984)041<0313:TEFOTT>2.0.CO;2.

Lau, W. K. M., and K.-M. Kim, 2012: The 2010 Pakistan Flood and Russian Heat Wave: Teleconnection of Hydrometeorological Extremes. *J. Hydrometeorol.*, doi:10.1175/JHM-D-11-016.1.

Luo, D., Y. Xiao, Y. Yao, A. Dai, I. Simmonds, and C. L. E. Franzke, 2016: Impact of ural blocking on winter warm Arctic-cold Eurasian anomalies. Part I: Blocking-induced amplification. *J. Clim.*, **29**, 3925-3947, doi:10.1175/JCLI-D-15-0611.1.

LUPO, A. R., and P. J. SMITH, 1995: Climatological features of blocking anticyclones in the Northern Hemisphere. *Tellus A*, doi:10.1034/j.1600-0870.1995.t01-3-00004.x.

Ma, S., C. Zhu, S. Ma, and C. Zhu, 2018: Extreme cold wave over East Asia in January 2016: A possible response to the larger internal atmospheric variability induced by Arctic warming. *J. Clim.*, JCLI-D-18-0234.1, doi:10.1175/JCLI-D-18-0234.1. http://journals.ametsoc.org/doi/10.1175/JCLI-D-18-0234.1.

Masato, G., B. J. Hoskins, and T. Woollings, 2013: Winter and Summer Northern Hemisphere Blocking in CMIP5 Models. *J. Clim.*, doi:10.1175/JCLI-D-12-00466.1.

Matsueda, M., 2011: Predictability of Euro-Russian blocking in summer of 2010. *Geophys. Res. Lett.*, **38**, 1-6, doi:10.1029/2010GL046557.

Mukougawa, H. and Sato, H. (1999). Multiple Weather Regimes in the Summertime North Atlantic Circulation. *J. Meteorol. Soc. Japan,* **77(2),** 483-494

Nakamura, H., M. Nakamura, and J. L. Anderson, 1997: The Role of High- and Low-Frequency Dynamics in Blocking Formation. *Mon. Weather Rev.*, doi:10.1175/1520-0493(1997)125<2074:TROHAL>2.0.CO;2.

_____, and T. Fukamachi, 2004: Evolution and dynamics of summertime blocking over the Far East and the associated surface Okhotsk high. *Q. J. R. Meteorol. Soc.*, doi:10.1256/qj.03.101.

Nakamura, N., and C. S. Y. Huang, 2018: Atmospheric blocking as a traffic jam in the jet stream. *Science (80-.).*, doi:10.1126/science.aat0721.

Pelly, J. L., and B. J. Hoskins, 2003: A New Perspective on Blocking. *J. Atmos. Sci.*, doi:10.1175/1520-0469(2003)060<0743:ANPOB>2.0.CO;2.

Renwick, J. A., and J. M. Wallace, 1996: Relationships between North Pacific Wintertime Blocking, El Niño, and the PNA Pattern. *Mon. Weather Rev.*, doi:10.1175/1520-0493(1996)124<2071:RBNPWB>2.0.CO;2.

REX, D. F., 1950: Blocking Action in the Middle Troposphere and its Effect upon Regional Climate. *Tellus*, doi:10.3402/tellusa.v2i4.8603.

Schaller, N., J. Sillmann, J. Anstey, E. M. Fischer, C. M. Grams, and S. Russo, 2018: Influence of blocking on Northern European and Western Russian heatwaves in large climate model ensembles. *Environ. Res. Lett.*, doi:10.1088/1748-9326/aaba55.

Shabbar, A., J. Huang, and K. Higuchi, 2001: The relationship between the wintertime North Atlantic oscillation and blocking episodes in the North Atlantic. *Int. J. Climatol.*, doi:10.1002/joc.612.

Shutts, G. J., 1983: The propagation of eddies in diffluent jetstreams: Eddy vorticity forcing of 'blocking' flow fields. *Q. J. R. Meteorol. Soc.*, doi:10.1002/qj.49710946204.

_____, 1986: A case study of eddy forcing during an atlantic blocking episode. *Adv. Geophys.*, doi:10.1016/S0065-2687(08)60037-0.

Singh, D., D. L. Swain, J. S. Mankin, D. E. Horton, L. N. Thomas, B. Rajaratnam, and N. S. Diffenbaugh, 2016: Recent amplification of the North American winter temperature dipole. *J. Geophys. Res.*, **121**, 9911-9928, doi:10.1002/2016JD025116.

Swanson, K. L., 2001: Blocking as a local instability to zonally varying flows. *Q. J. R. Meteorol. Soc.*, **127**, 1341-1355, doi:10.1256/smsqj.57411.

TIBALDI, S., and F. MOLTENI, 1990: On the operational predictability of blocking. *Tellus A*, doi:10.1034/j.1600-0870.1990.t01-2-00003.x.

Traction, M. S., 1990: Predictability and its relationship to scale interaction processes in blocking. *Mon. Weather Rev.,* **118,** 1666-1695

Trigo, R. M., I. F. Trigo, C. C. DaCamara, and T. J. Osborn, 2004: Climate impact of the European winter blocking episodes from the NCEP/NCAR reanalyses. *Clim. Dyn.*, doi:10.1007/s00382-004-0410-4.

TSOU, C. -H, and P. J. SMITH, 1990: The role of synoptic/planetary-scale interactions during the development of

a blocking anticyclone. *Tellus A*, **42**, 174-193, doi:10.1034/j.1600-0870.1990.00015.x.

Wang, S. Y. S., W. R. Huang, and J. H. Yoon, 2015: The North American winter 'dipole' and extremes activity: A CMIP5 assessment. *Atmos. Sci. Lett.*, **16**, 338-345, doi:10.1002/asl2.565.

Woollings, T., and Coauthors, 2018: Blocking and its Response to Climate Change. *Curr. Clim. Chang. Reports*, doi:10.1007/s40641-018-0108-z.

_____, B. Hoskins, M. Blackburn, and P. Berrisford, 2008: A New Rossby Wave-Breaking Interpretation of the North Atlantic Oscillation. *J. Atmos. Sci.*, doi:10.1175/2007JAS2347.1.

Yao, Y., D. Luo, A. Dai, and I. Simmonds, 2017: Increased quasi stationarity and persistence of winter ural blocking and Eurasian extreme cold events in response to arctic warming. Part I: Insights from observational analyses. *J. Clim.*, doi:10.1175/JCLI-D-16-0261.1.

Table 1. Abbreviations of the forcing terms in Eq. (11) decomposed by transient eddies and its tendency

Tendency	Transient eddy forcing	
χ_{HF}^{vort}	$-\nabla \cdot (V_{HF}\zeta_{HF} + V_{HF}f)$	High−frequency absolute vorticity forcing term
$\chi_{HF\_R}^{vort}$	$-\nabla \cdot V_{HF}\zeta_{HF}$	High−frequency relative vorticity forcing term
$\chi_{HF\_P}^{vort}$	$-\nabla \cdot V_{HF}f$	High−frequency planetary vorticity forcing term
χ_{CF}^{vort}	$-\nabla \cdot (V_{LF}\zeta_{HF} + V_{HF}\zeta_{LF})$	Cross−frequency relative vorticity forcing term
χ_{CF1}^{vort}	$-\nabla \cdot V_{LF}\zeta_{HF}$	Cross−frequency relative vorticity forcing term associate with large−scale background wind
χ_{CF2}^{vort}	$-\nabla \cdot V_{HF}\zeta_{LF}$	Cross−frequency relative vorticity forcing term associate with synoptic−scale flows
χ_{LF}^{vort}	$-\nabla \cdot (V_{LF}\zeta_{LF} + V_{LF}f)$	Low−frequency absolute vorticity forcing term
$\chi_{LF\_R}^{vort}$	$-\nabla \cdot V_{LF}\zeta_{LF}$	Low−frequency relative vorticity forcing term
$\chi_{LF\_P}^{vort}$	$-\nabla \cdot V_{LF}f$	Low−frequency planetary vorticity forcing term

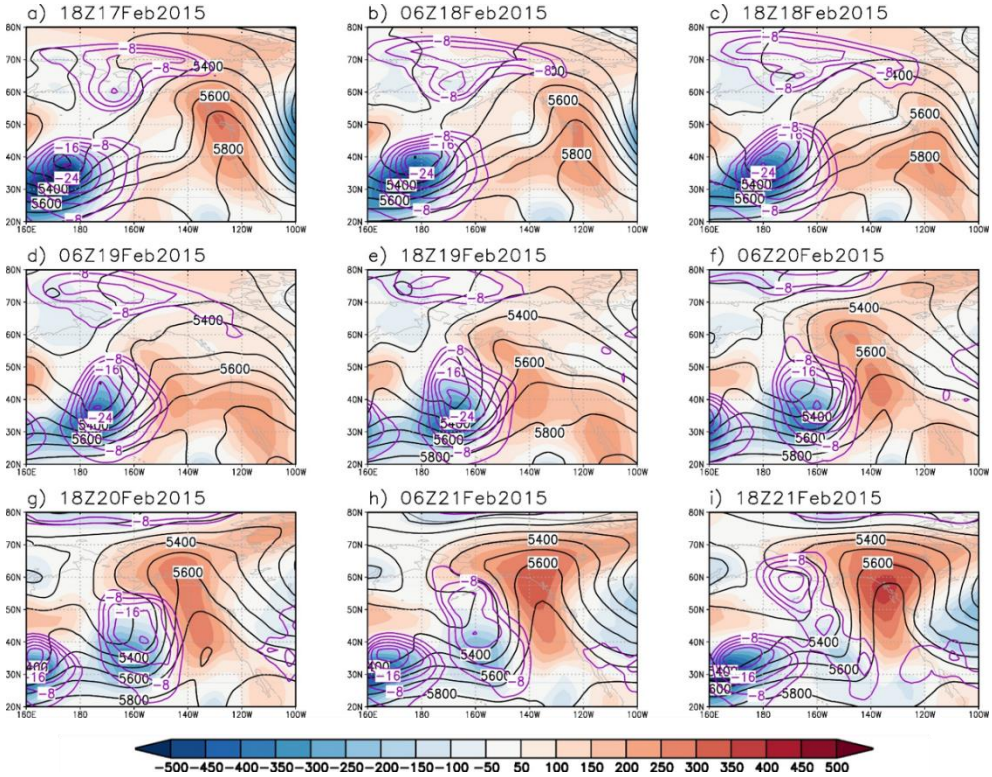

Figure 1. Time evolution of blocking that occurred on February 21, 1800 UTC in 2015. Shading shows the geopotential height anomaly of the Z500 fields (gpm). The black contour shows Z500 lines (gpm), and the purple contour shows a negative sea−level pressure anomaly (hPa).

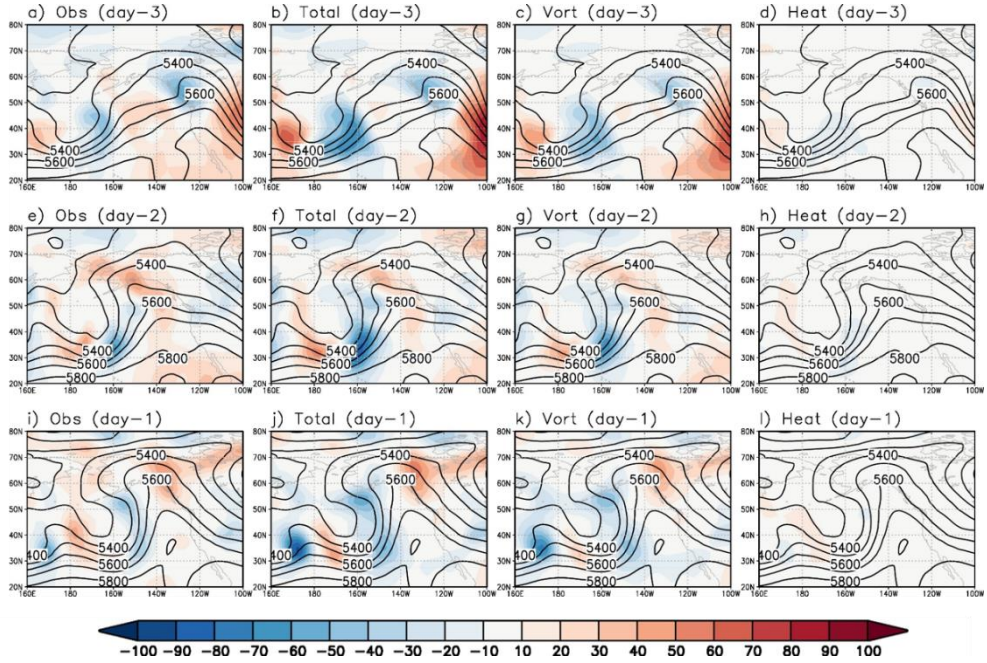

Figure 2. . Quasigeostrophic height tendency (m/6 h) for 1800 UTC 18 February 2015 and 1800 UTC 20 February 2015. The black contour shows Z500 fields (gpm).

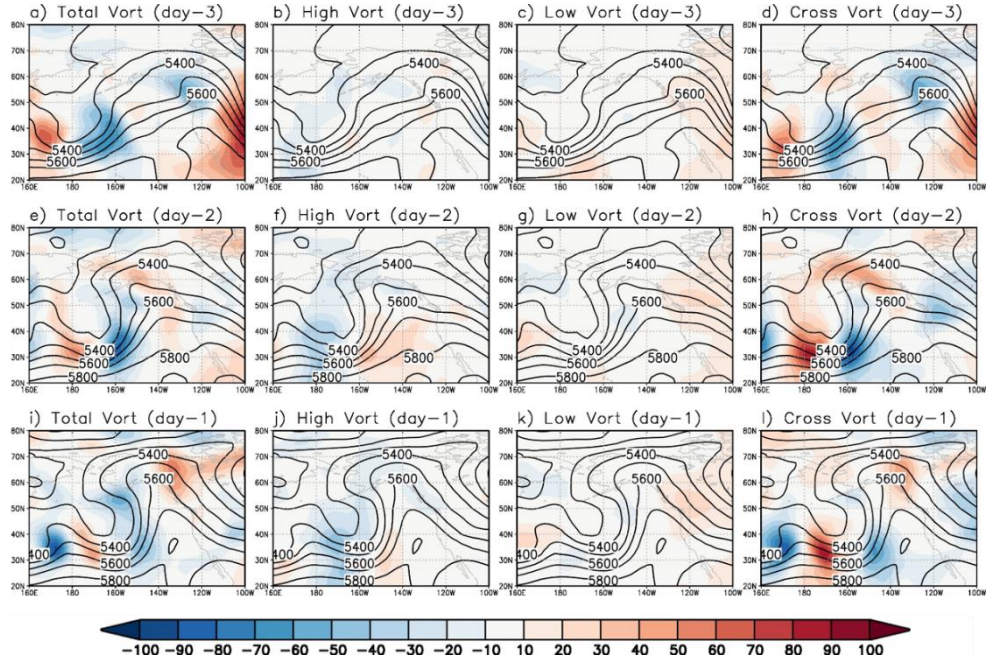

Figure 3. Quasigeostrophic height tendency (m/6 h) obtained by transient eddy vorticity forcing for 1800 UTC 18 February 2015 and 1800 UTC 20 February 2015. The black contour shows Z500 fields (gpm).

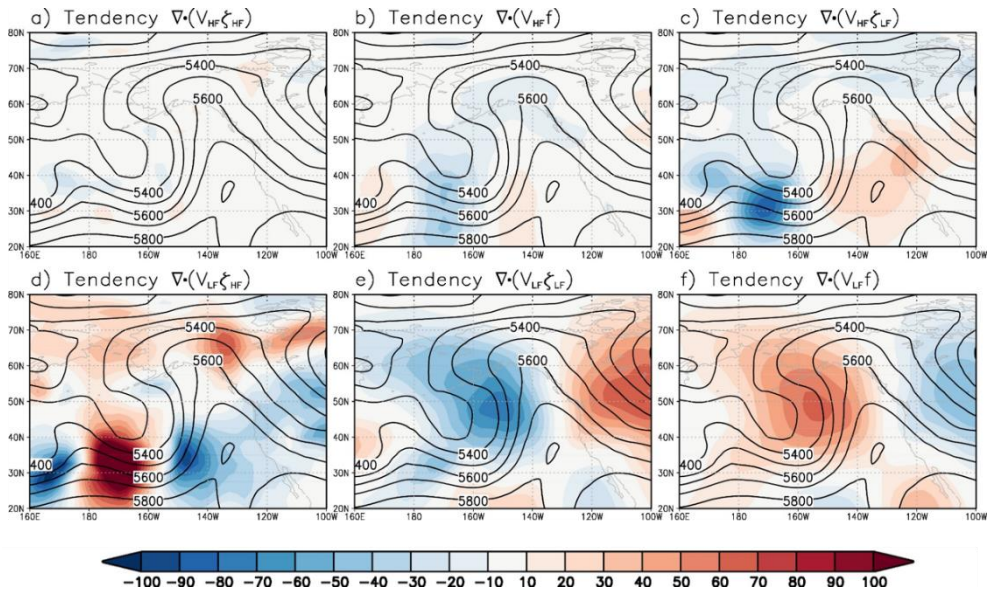

Figure 4. Quasigeostrophic height tendency (m/6 h) obtained by the transient eddy relative forcing and planetary vorticity forcing on 1800 UTC 20 February 2015. The unit is m/6 h, and the black contour shows Z500 fields (gpm).

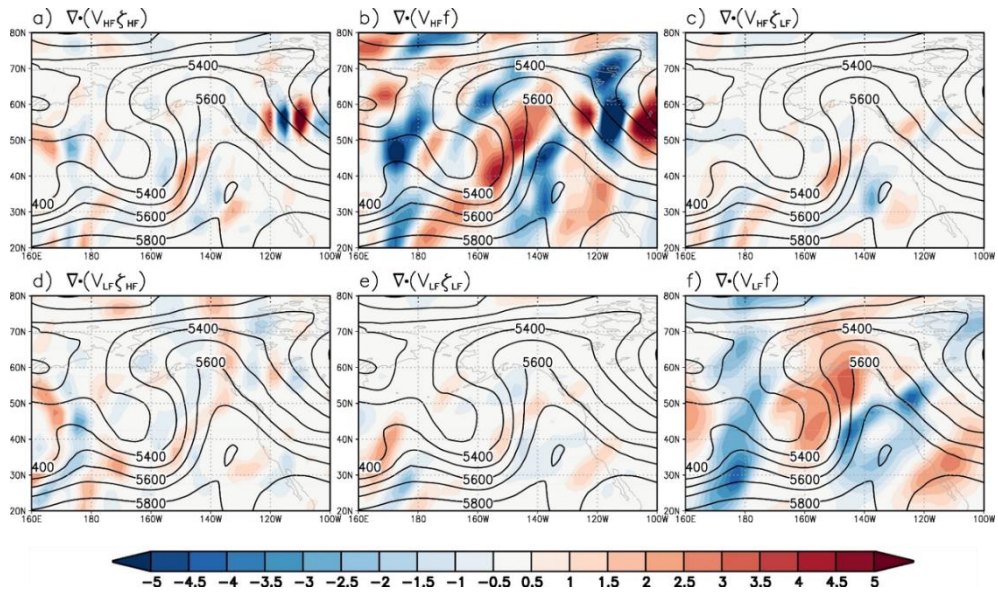

Figure 5. Transient eddy relative forcing and planetary vorticity forcing (s^{-2}) on 1800 UTC 20 February 2015. The black contour shows Z500 fields (gpm).

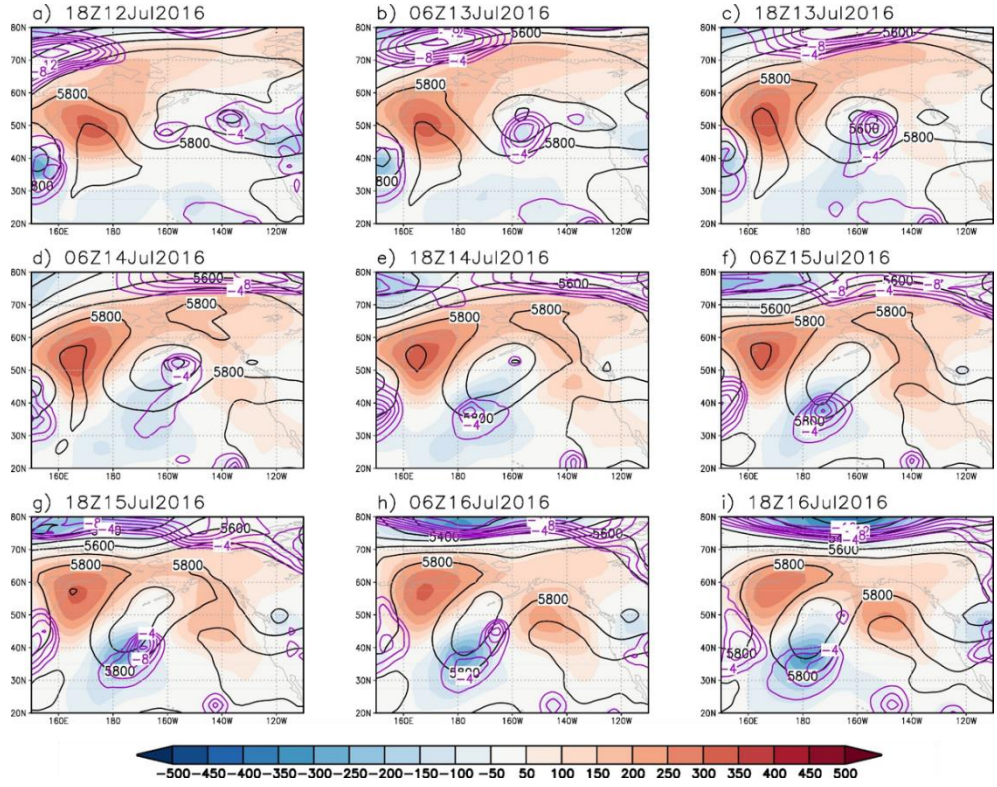

Figure 6. Same as Figure 1 but for the summer blocking, which occurred at 1800 UTC 16 July 2016.

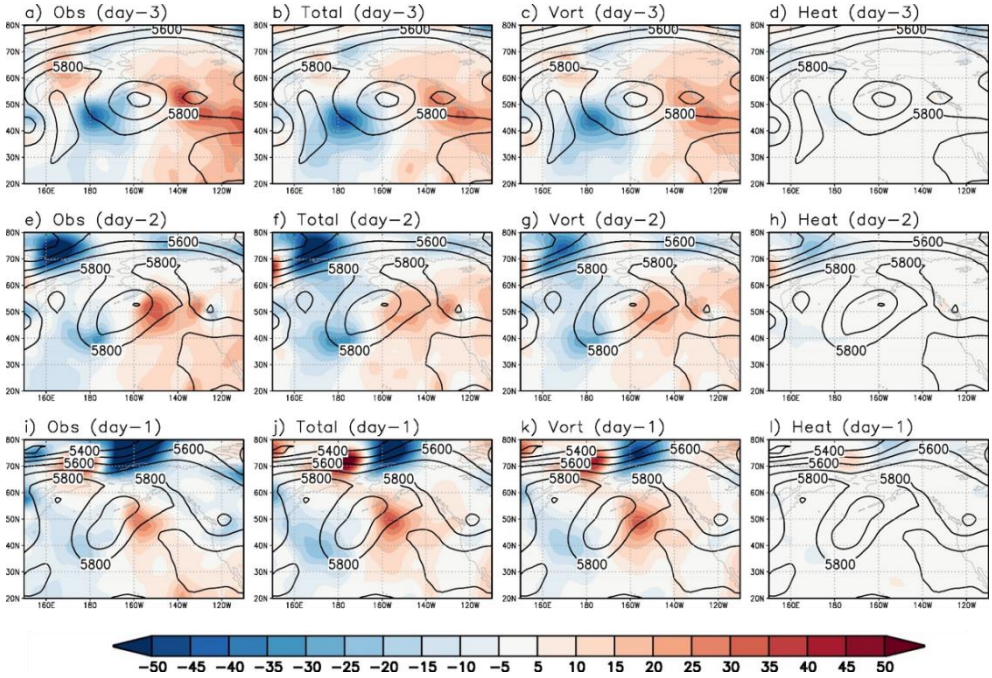

Figure 7. Same as Figure 2 but for 1800 UTC 13 July 2016 and 1800 UTC 15 July 2016.

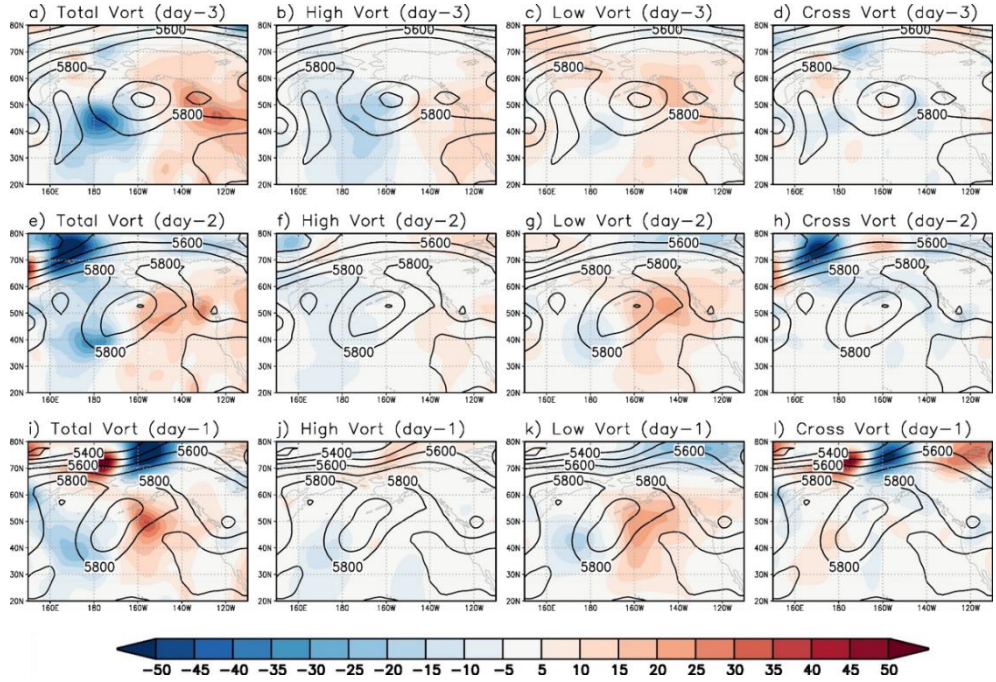

Figure 8. Same as Figure 3 but for 1800 UTC 13 July 2016 and 1800 UTC 15 July 2016.

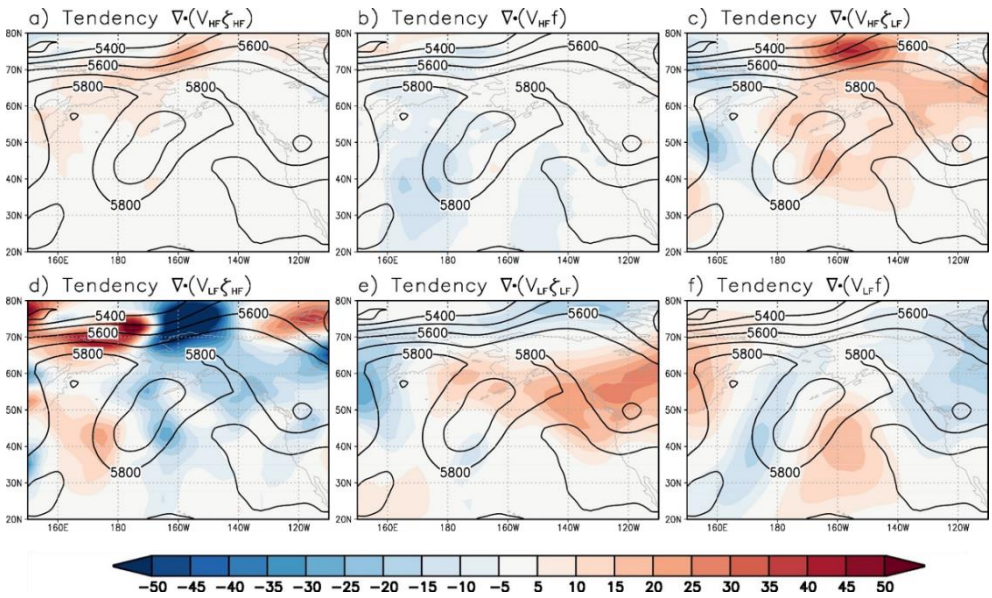

Figure 9. Same as Figure 4 but for 1800 UTC 15 July 2016.

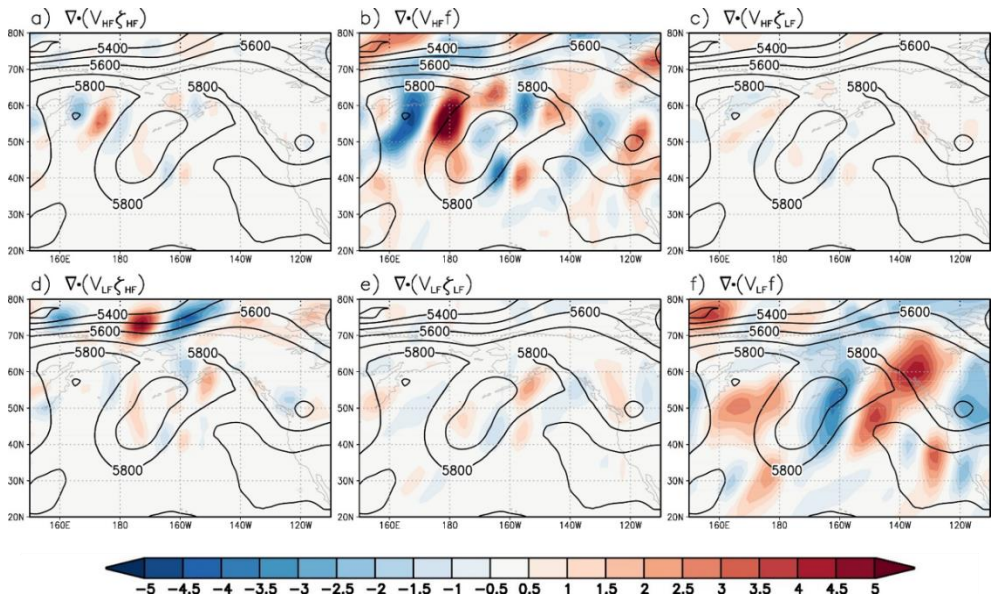

Figure 10. Same as Figure 5 but for 1800 UTC 15 July 2016.

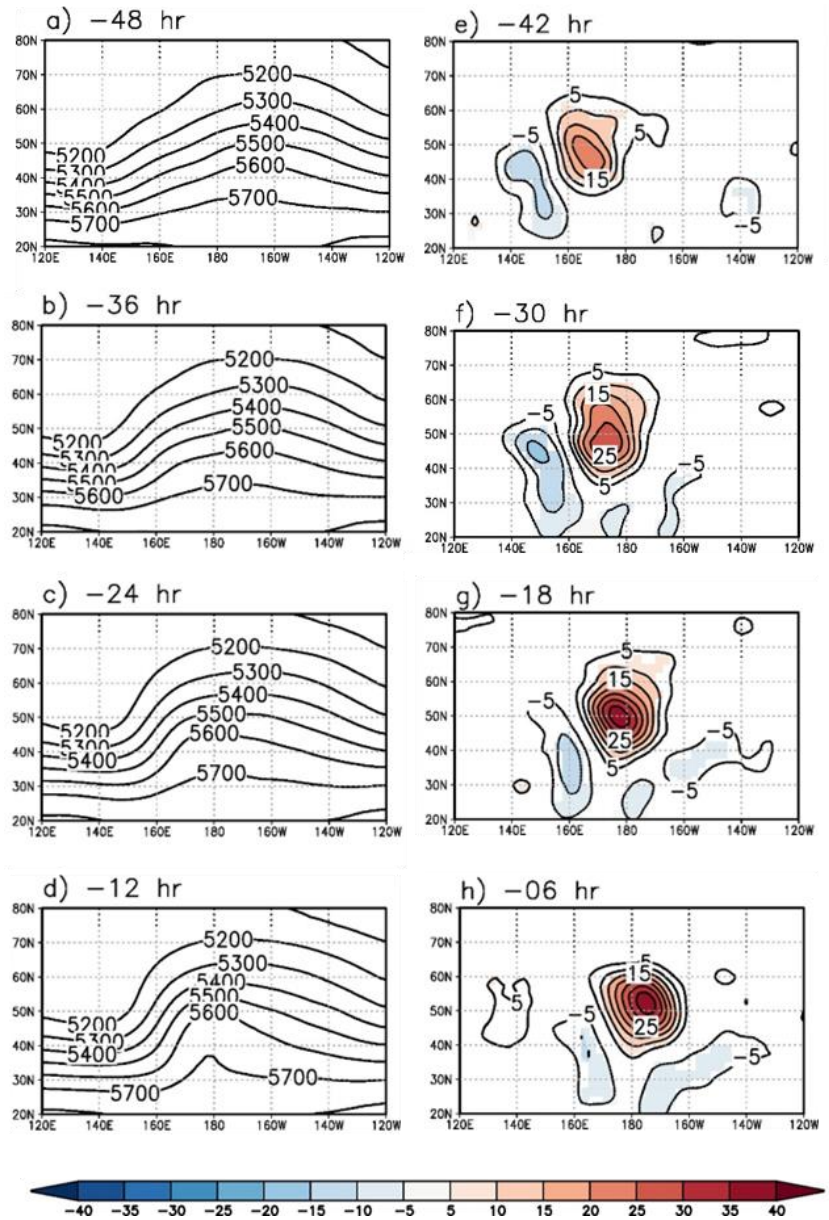

Figure 11. . Composite: time evolution of Z500 fields (gpm) and geopotential height tendency (m/6 h) associated with Pacific blocking in winter. Shaded areas are statistically significant areas in geopotential height tendency at the 95% confidence level from zero.

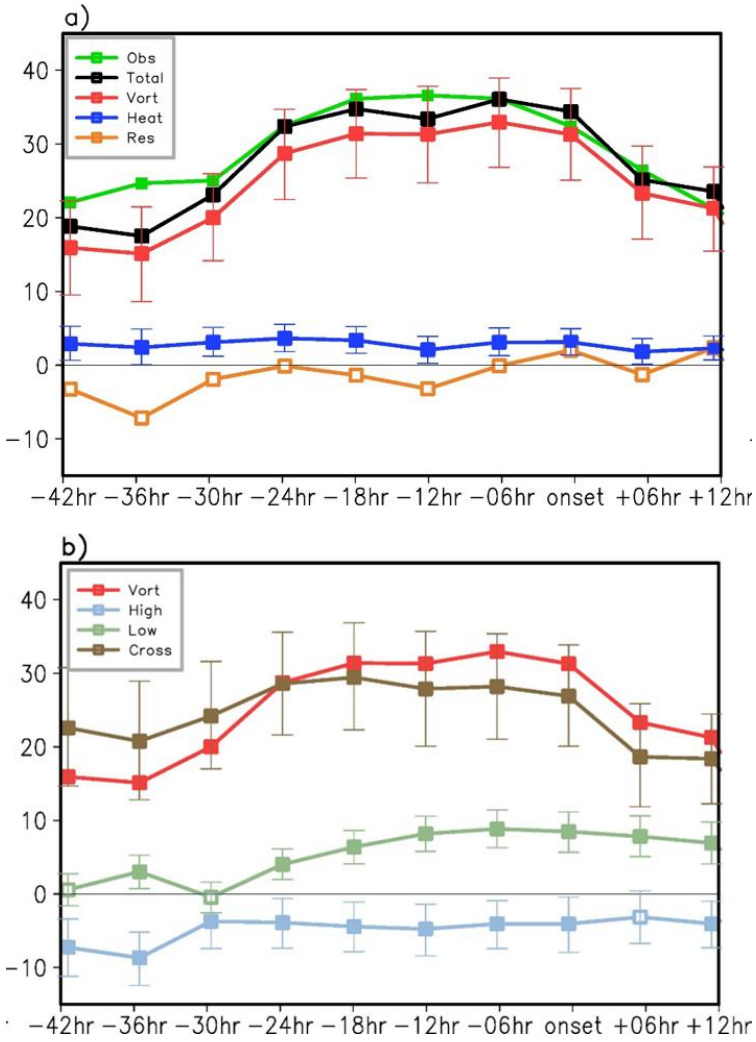

Figure 12. Time evolution of geopotential height tendency of budget analysis at the center of winter blockings. Top: observations (green), total (black), vorticity flux (blue), and heat flux (red). The orange line represents a residual between the observations and total budget. Bottom: total (red), low-frequency transient eddy forcing (light-green), cross-frequency eddy forcing (brown), and high-frequency transient eddy forcing (sky). The error bars show the 95% confidence interval of the mean values. The marked line shows statistical significance from zero.

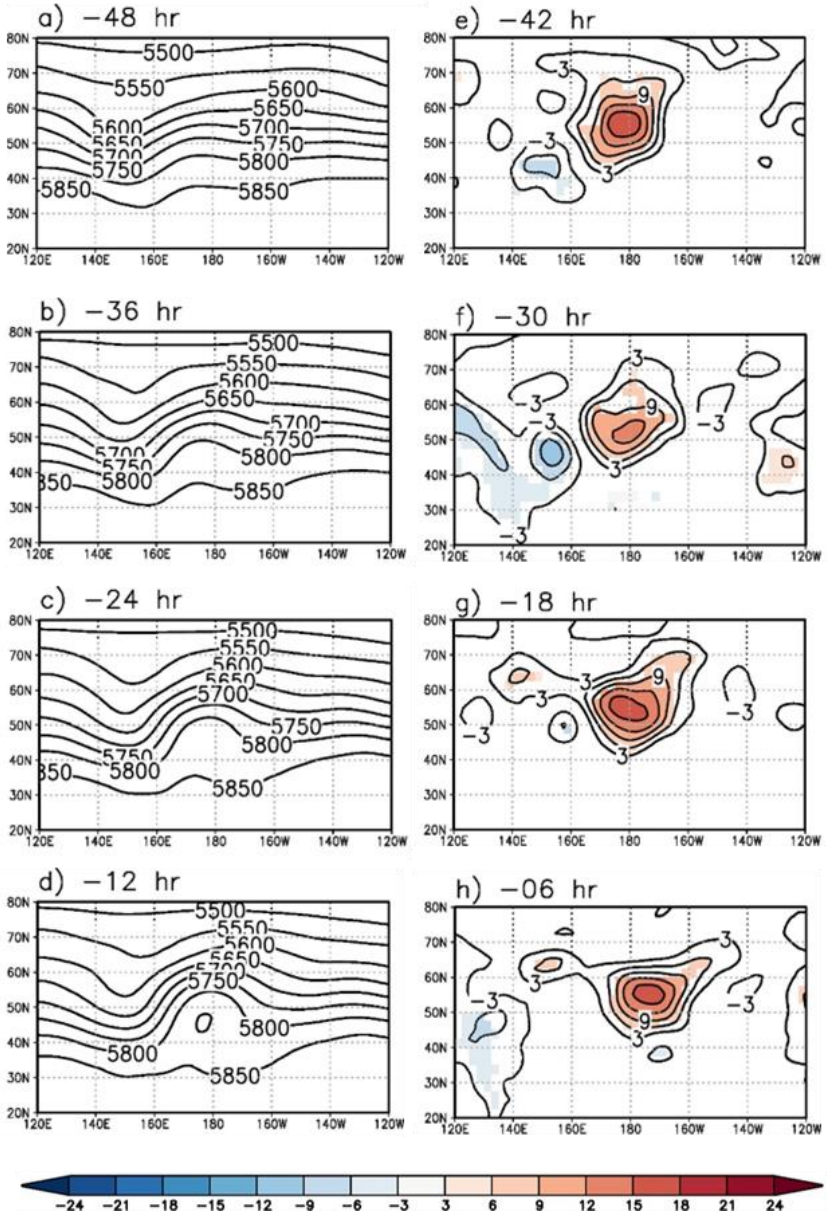

Figure 13. As for Figure 11, but for the summer blockings

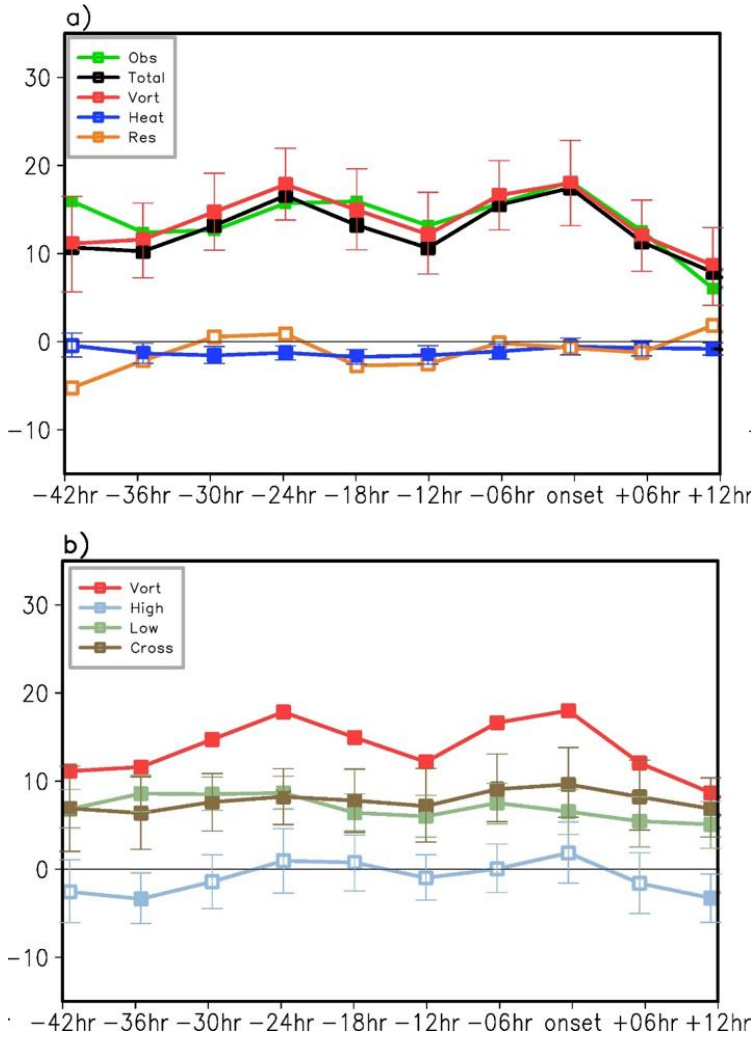

Figure 14. As for Figure 12, but for the summer blockings

초 록

태평양 블로킹 형성에서의 일시 에디의 역할

황 재 영
지구환경과학부
석사과정
서울대학교

태평양 블로킹 형성 과정을 준-지균 지위고도 경향 방정식의 수지분석을 이용하여 정량적으로 조사하고자 하였다. 겨울철 사례분석의 경우 블로킹 발생 지역의 상류 지역에서 강한 저기압이 존재하였고, 이 저기압과 기존에 발달 되어있는 능선과의 역학적 관계를 통해서 블로킹이 성장하는 것을 확인할 수 있었다. 여름철 사례분석의 경우 기존에 존재하던 블로킹에 의해 새로운 블로킹이 발달하는 것을 확인할 수 있었다. 두 사례 분석을 준-지균 지위고도 경향 방정식을 통해서 살펴본 결과 두 사례 분석 모두 태평양 블로킹 형성과 관련된 지위고도 경향은 소용돌이 도속의 발산항에 의해 대부분 설명이 가능함을 확인하였다. 소용돌이속 발산항을 고주파 및 저주파 일시 에디항으로 나누어서 이들의 기여도를 확인해 보았을 때, 겨울철 블로킹 사례에서는 교차주파 일시 에디항으로

이루어진 소용돌이속 발산항이 블로킹 형성의 대부분을 설명하였다. 특히 교차주파 일시 에디항 중 저주파 수평속도 항과 고주파 소용돌이도항의 상호작용이 블로킹 형성과 깊은 관련이 있을 것으로 확인이 되었다. 반면 여름철 사례분석의 경우 저주파 소용돌이도속에 의한 지위고도 경향이 블로킹 형성과 깊은 관련이 있는 것으로 조사 되었다. 각 각의 계절에서 발생한 블로킹의 합성장 분석을 실시한 결과, 겨울철 및 여름철 모두 사례분석과 동일하게 태평양 블로킹 형성과 관련된 지위고도 경향은 소용돌이도속 발산항과 연관이 있는 것으로 나타났다. 겨울철의 경우 사례분석과 마찬가지로 교차주파 일시 에디항으로 이루어진 소용돌이속 발산항이 블로킹 형성에 지배적인 역할을 하는 것으로 나왔다. 반면 여름철에서는 교차주파 일시 에디항으로 이루어진 소용돌이속 발산항과 저주파 일시 에디항으로 소용돌이속 발산항의 기여도가 비슷한 것으로 나타났다. 이는 여름철 블로킹 형성의 경우 겨울철 블로킹 형성 기작과 다른 기작으로 발생하는 블로킹의 존재를 암시한다.

주요어 : 블로킹, 일시 에디, 준-지균 지위고도 경향 방정식

Student Number : 2016-23149